

SECURITY OF FACIAL FORENSICS MODELS AGAINST ADVERSARIAL ATTACKS

Rong Huang¹, Fuming Fang², Huy H. Nguyen³, Junichi Yamagishi^{2,3}, Isao Echizen^{2,3}

¹College of Information Science and Technology, Donghua University, Shanghai, China

²National Institute of Informatics, Tokyo, Japan

³SOKENDAI (The Graduate University for Advanced Studies), Kanagawa, Japan

ABSTRACT

Deep neural networks (DNNs) have been used in digital forensics to identify fake facial images. We investigated several DNN-based forgery forensics models (FFMs) to examine whether they are secure against adversarial attacks. We experimentally demonstrated the existence of individual adversarial perturbations (IAPs) and universal adversarial perturbations (UAPs) that can lead a well-performed FFM to misbehave. Based on iterative procedure, gradient information is used to generate two kinds of IAPs that can be used to fabricate classification and segmentation outputs. In contrast, UAPs are generated on the basis of over-firing. We designed a new objective function that encourages neurons to over-fire, which makes UAP generation feasible even without using training data. Experiments demonstrated the transferability of UAPs across unseen datasets and unseen FFMs. Moreover, we conducted subjective assessment for imperceptibility of the adversarial perturbations, revealing that the crafted UAPs are visually negligible. These findings provide a baseline for evaluating the adversarial security of FFMs.

Index Terms— forgery forensics, adversarial attack, over-firing

1. INTRODUCTION

Faces appearing in digital media are salient information that directly reflects personal identity and scene content. Facial manipulation programs, like DeepFakes [1], Face2Face and FaceSwap [2], can be used to automatically edit facial identities and expressions so as to alter the semantic content of the digital media. To deal with this security threat, many countermeasures [3–12] have been proposed. Inspired by presentation attack detection, researchers are attempting to use liveness clues like lip-syncing [3], eye blinking [4], and inconsistency in head pose [5] to identify fake facial videos. Another approach is to use inconsistent statistical characteristics including IQM (image quality metrics) descriptor [6], color disparity [7], and warping artifacts [8] as telltale indicators for detecting forgeries. DNNs have also been used to expose fake facial media [9, 10]. To enhance transferability, Cozzolino *et al.* [11] designed a selection-based domain adaptation mechanism over the latent space of an autoencoder. A variation of this approach [12], using a multi-task autoencoder, was proposed for simultaneously achieving the forensic goals of forgery identification and localization. The reported DNN-based FFMs [9–12] have exhibited outstanding performance and shown great potential in security-sensitive intelligent systems, such as fake news identification and electronic evidence investigation.

However, the security of these DNN-based FFMs [9–12] is problematic since an attacker may carefully fabricate a fake facial image or video to circumvent the intelligent systems for getting higher but illegal privilege. Recent works [13, 14] have revealed that adding a tailor-made tiny noise to the bona fide input can easily induce a well-performed DNN to produce misleading output. Previous works on adversarial attacks mainly focused on tasks involving face recognition [15], object detection [16], semantic segmentation [17], natural language processing [18], and malware detection [19]. There has been a lack of work on whether FFMs are secure against adversarial attacks. We aim to fill this gap, in this paper, by applying gradient-based adversarial attacks (white box) to Nguyen’s FFM [12] and evaluating the transferability of adversarial perturbations (black box) across unseen datasets and unseen FFMs [10, 11].

Specifically, our contributions are as follows: **1.** We show the existence of IAPs, which can be used to fabricate classification or segmentation outputs. **2.** We show the existence of image-agnostic UAPs for the FFM [12]. We present a newly designed objective function that enables latent neurons to be over-fired without the need for training data. **3.** We present experimental results demonstrating that UAPs have transferability across unseen datasets and unseen FFMs [10, 11]. **4.** Following an international standard [20], we conduct subjective assessment for imperceptibility of adversarial perturbations. This is a necessary step oriented towards practical applications of the adversarial attack.

The experimental results presented in Section 3 support the above claims and thereby demonstrate that existing FFMs [10–12] are vulnerable to adversarial attacks. This work provides a warning that future digital forensics research should take into account the need to integrate an adversarial defense mechanism into FFMs.

2. BACKGROUND

In this section, we give a brief introduction of the target facial FFMs [10–12], and then introduce fundamental concepts and impressive achievements in the field of adversarial attack.

2.1. Target FFMs

In [10], Afchar *et al.* constructed a lightweight DNN with four convolutional layers and two fully connected layers, and furthermore proposed an advanced network structure called ‘MesoInception-4’. Inception modules consisting of vanilla convolutions, dilated convolutions and skip-connections (1×1 convolutions) were introduced for adaptively probing low-level image textures.

The ForensicTransfer method [11] is based on an autoencoder architecture. For a given image x_i , its residual map that only contains high-frequency details is regarded as the input. Neurons in the latent layer are divided equally into two disjoint portions: zero zone

This work was partially supported by a JST CREST Grant (JP-MJCR18A6, VoicePersonae project), Japan, and by MEXT KAKENHI Grants (16H06302, 17H04687, 18H04120, 18H04112, 18KT0051), Japan.

$h_{i,0}$ and one zone $h_{i,1}$. The zone-wise activation energy is calculated by $a_{i,c} = \|h_{i,c}\|_1/K_c$, where K_c counts the number of neurons in the c^{th} zone for $c \in \{0, 1\}$. The activation loss for an image x_i is defined as $\mathcal{L}_{\text{act}}(x_i, l_i) = |a_{i,1} - l_i| + |a_{i,0} - (1 - l_i)|$, where l_i represents the category label, which takes the value 0 for ‘fake’ and 1 for ‘real’. The activation loss encourages the zone $h_{i,c}$ that $c = l_i$ to activate ($a_{i,c} > 0$) while the other zone $h_{i,1-c}$ remains silent ($a_{i,1-c} = 0$). During the training phase, the selection module compulsively zeros out the off-class zone $h_{i,1-c}$, which forces the decoder to complete its reconstruction task using only $h_{i,c}$. During the testing phase, an image x_i is classified as c if $a_{i,c} > a_{i,1-c}$. This encoder-selection-decoder framework forces the latent space to learn discriminative representations and thus enhances the transferability across multiple domains of image manipulations.

In [12], Nguyen *et al.* proposed a Y-shaped network that extends the network of Cozzolino *et al.* [11] in three ways. First, the residual module is abandoned so that a variety of features can be adaptively probed by convolutional layers without constraints. Second, the autoencoder architecture is made deeper (with up to 18 convolutional layers). Third, the decoder is designed as a two-pronged structure, which enables three tasks (classification, segmentation, and reconstruction) to share the information they learn and thereby enhance overall performance. The segmentation branch is responsible for locating forged regions. Cross-entropy loss $\mathcal{L}_{\text{seg}}(x_i, m_i)$ is used to evaluate the segmentation quality, where m_i represents the ground-truth mask.

In this paper, the above three representative FFMs [10–12] are considered as the target models for examining the existence and effectiveness of adversarial perturbations. FaceForensics++ database [21] was used to train or fine-tune the three FFMs. It consists of three datasets, ‘DeepFakes’, ‘Face2Face’ and ‘FaceSwap’. Each dataset contains 1000 real facial videos and 1000 manipulated ones. This database also provides ground-truth masks that highlight the manipulated regions in a pixel-wise manner. Data preparation followed the procedure previously used in [11, 12], so there were 2800 images in each test set that would be used to evaluate the performance of adversarial attacks.

2.2. Adversarial Attacks

Given an image x_i and a target model f , an adversarial attack aims to find a tiny perturbation, denoted by ξ_i , so that the corresponding adversarial image $x_i^{\text{adv}} = x_i + \xi_i$ can change the output of f , i.e., $f(x_i) \neq f(x_i^{\text{adv}})$. During the course of seeking ξ_i , its magnitude, which is usually measured by the p -norm distance, is bounded by a small value to ensure its imperceptibility.

In the pioneering work [22], Szegedy *et al.* generated adversarial perturbations by using a box-constrained L-BFGS. However, this method is relatively time-consuming. A suitable value of hyperparameter c that modulates the balance between two terms in the objective function is unknown. This therefore requires an additional line-searching to adaptively update c .

Fast gradient sign method (FGSM) proposed by Goodfellow *et al.* [23] is an efficient one-time method without iterations. An adversarial image is generated by slightly adapting each pixel along the direction of the sign of gradient. Basic iterative method (BIM) [24] is an intuitive extension of FGSM. It iteratively generates an adversarial perturbation with a smaller step size, which enables the updating direction to be adjusted after each iteration.

Deepfool [25] was proposed for finding a minimal perturbation ξ_i that could just push x_i outside its own classification region. An iterative procedure is used to gradually estimate ξ_i under the assumption that the linearity of f holds around x_i at each iteration.

In [26], Moosavi-Dezfooli *et al.* leveraged the Deepfool method to craft an image-agnostic UAP Ξ that can fool the target model f , i.e., $f(x_i) \neq f(x_i + \Xi)$, for a vast majority of x_i . The crafted UAP was empirically demonstrated to transfer well across multiple architectures including VGG, CaffeNet, GoogLeNet, and ResNet.

The idea of Mopuri *et al.*’s work [27] is to seek a UAP that can over-fire the neurons (maximizing the activation energies) at each layer. Such a UAP would contaminate the learned features and thereby lead the target model to misbehave. Particularly interesting is that the training phase for over-firing can be done in a data-free manner.

In this paper, the gradient information itself (rather than the signed version) was used for generating IAPs. Inspired by the idea of over-firing, we crafted UAPs without using training data. However, we found that, for autoencoder network [12], it is difficult to achieve over-firing due to the small magnitude of the perturbation-only input. We solved this problem by designing a new objective function that strongly promotes over-firing of the latent neurons in the desired zone (see Section 3.2).

3. ADVERSARIAL PERTURBATIONS FOR FFMS

In this section, we mount the adversarial attacks against the FFM [12] for different falsification purposes. First, we craft two kinds of IAPs for each image, one for fabricating classification output and one for fabricating segmentation output. Next, we craft UAPs in accordance with the idea of over-firing and evaluate their transferability across unseen datasets and unseen FFMs [10, 11]. Finally, we describe the settings for the subjective assessment and summarize the insights gained from the assessment into the imperceptibility of adversarial perturbations.

3.1. Individual adversarial attacks

Given an image x_i , we iteratively generate a tailor-made IAP that can flip the original classification output. The iterative procedure can be written as:

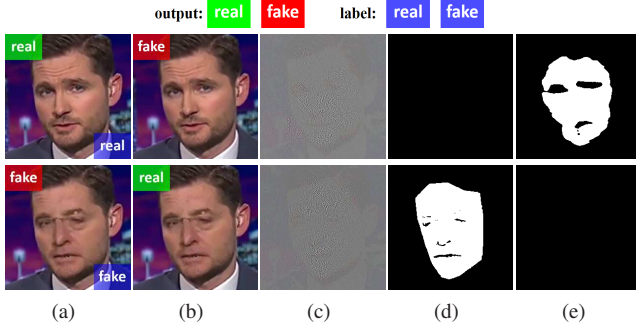
$$\xi_i^{(n+1)} = \text{Clip}_\epsilon \left\{ \xi_i^{(n)} - \alpha (\nabla_{x_i} \mathcal{L}_{\text{act}}(x_i + \xi_i^{(n)}, l_i^{\text{adv}})) \right\}, \quad (1)$$

where $\xi_i^{(n)}$ denotes the adversarial perturbation at the n^{th} iteration while α represents the step size. The iterative procedure starts with $\xi_i^{(0)} = \mathbf{0}$. At each iteration, the operator $\text{Clip}_\epsilon(\cdot)$ restricts the perturbation’s magnitude within $[-\epsilon, \epsilon]$ to ensure imperceptibility. Adversarial label l_i^{adv} satisfying $l_i^{\text{adv}} \neq l_i$ enables the fabricated output to be controlled. For a binary classification problem (‘real’ or ‘fake’), it is easy to prepare the adversarial label: $l_i^{\text{adv}} = 1 - l_i$. The sign operator previously used in FGSM and BIM is excluded from our iterative procedure since we consider that not only the direction but also the length of the gradient is informative in generating IAPs. Note that only the activation loss is used in Eq.(1) because the classification is performed in accordance with the zone-wise activation energy. We set $\alpha = 1.0$ and $\epsilon = 2.5$ throughout our experiments.

Table 1 shows that adding IAPs drastically reduced classification accuracies. The small RMSE (root mean squared error) scores, however, suggest perceptual similarities between x_i and x_i^{adv} . More importantly, 20 iterations for each image were sufficient to destroy the well-performed FFM [12] over the three datasets. Furthermore, the Intersection-over-Union (IoU) scores were dramatically suppressed at the same time although the segmentation loss $\mathcal{L}_{\text{seg}}(x_i, m_i)$ was absent from the iterative procedure. This is because only activated latent features $h_{i,c}$ were selected for the following decoder, so the classification output greatly affected the segmentation branch.

Table 1. Performance of IAPs (fabricating classification outputs).

dataset	setting	acc (%)	IoU (%)	RMSE
DeepFakes	original	94.79	63.28	-
	10 iters	0.00	0.02	1.25
	20 iters	0.00	0.02	1.27
Face2Face	original	91.86	69.10	-
	10 iters	0.35	0.15	1.41
	20 iters	0.00	0.00	1.50
FaceSwap	original	89.29	62.36	-
	10 iters	0.75	0.37	1.38
	20 iters	0.00	0.00	1.45

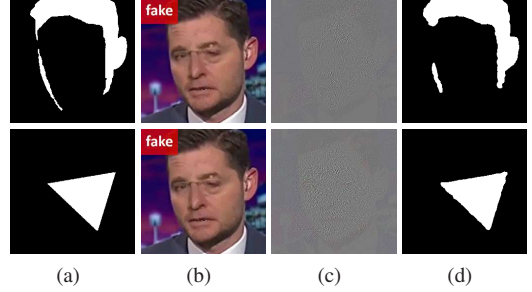
**Fig. 1.** Resulting examples (selected from: FaceSwap & 20 iters). (a) Original images. (b) Adversarial images. (c) Adversarial perturbations (min-max scaled for display). (d) Ground-truth masks. (e) Segmentation outputs.

This phenomenon is reflected in the two resulting examples shown in Fig.1, in which the segmentation outputs, i.e., the column (e), agree with the fabricated classification outputs.

We also purposely fabricate incorrect segmentation outputs for fake images to mislead tampering localization judgement. In this scenario, the adversarial ground-truth masks m_i^{adv} , as shown in Fig.2 (a), are prepared in advance. The goal is to slightly adapt the pixels of x_i , making segmentation output as similar as possible to m_i^{adv} . To this end, we define a weighted objective function $\mathcal{L} = \mathcal{L}_{\text{act}}(x_i, l_i^{\text{adv}}) + \lambda \cdot \mathcal{L}_{\text{seg}}(x_i, m_i^{\text{adv}})$, where λ is set to 1.8 empirically. Then, this objective function is substituted into Eq.(1) for iterative computations. Here, the adversarial label l_i^{adv} is assigned a value close to but less than 0.5 (for example 0.45)¹ in this scenario. Such a setting loosens the interaction between classification and segmentation, while still ensuring that the zero zone $h_{0,i}$ is activated.

Figure 2 shows the corresponding resulting examples. Obviously, the fabricated masks (d) closely match the adversarial ones (a), and are much different from the original ones. For quantitative evaluation, it is time-consuming to manually create a meaningful adversarial mask for every image. For a quick experiment, we assume that an adversarial mask follows a simple geometry, i.e., a triangle, as shown by the bottom image in Fig.2 (a). The location and orientation of the triangle are randomly assigned for each image. The results of the quantitative evaluation are summarized in Table 2. The IoU scores w.r.t the adversarial masks were as high as 48.52% while those w.r.t the original masks were reduced on average from 43.21% to 22.04%. This means that adding IAPs leads the segmentation out-

¹Recall that label ‘fake’ takes the value 0 in this paper.

**Fig. 2.** Resulting examples (selected from: FaceSwap & 500 iters). (a) Adversarial mask. (b) Adversarial images. (c) Adversarial perturbations (min-max scaled for display). (d) Segmentation outputs. Original images and their ground-truth masks are shown in Fig.1.**Table 2.** Performance of IAPs (fabricating classification outputs). Only ‘fake’ images were considered in this scenario, so scores in the ‘original’ rows differ from those in Table 1.

dataset	setting	acc (%)	IoU (%) w.r.t		RMSE
			original mask	adversarial mask	
DeepFakes	original	96.79	47.20	-	-
	100 iters	97.71	6.16	45.36	1.46
	500 iters	99.93	30.93	48.37	1.53
Face2Face	original	85.07	40.06	-	-
	100 iters	99.14	24.13	45.72	1.65
	500 iters	100.00	23.50	48.22	1.70
FaceSwap	original	93.07	42.36	-	-
	100 iters	99.29	23.82	45.85	1.56
	500 iters	100.00	23.72	48.52	1.61

puts being more similar to the adversarial masks. It may be difficult to further reduce the IoU scores in this quick experiment because a triangle with a random location and orientation may partly overlap the original highlighted area. Interestingly, the classification accuracy got a rise in this scenario. This is because the setting $l_i^{\text{adv}} = 0.45$ forced the zero zone to activate, which provided a chance to correct previously misclassified outputs. In addition, fabricating a segmentation output needs 100 or more iterations, which has a higher computational cost than falsification for classification.

3.2. Universal adversarial attacks

In this scenario, we aim to craft a data-free UAP Ξ that can flip the classification outputs for most images. The iterative procedure starts with a random perturbation in which the entries obey a uniform distribution $[-\epsilon, \epsilon]$. For the autoencoder network [12], it is nontrivial to activate the latent neurons at the initial iterations due to the small magnitude of the perturbation-only input. To overcome this problem, we designed a new objective function:

$$\mathcal{L}(\Xi) = \exp\left(\frac{\kappa \cdot a_{i,1-c}}{a_{i,c}}\right) - a_{i,c}, \quad (2)$$

where $a_{i,c}$ and $a_{i,1-c}$ denote the activation energy of $h_{i,c}$ and $h_{i,1-c}$, respectively. The iterative procedure for updating Ξ can be formulated as

$$\Xi^{(n+1)} = \text{Clip}_\epsilon \{ \Xi^{(n)} - \alpha (\nabla \mathcal{L}(\Xi^{(n)})) \}. \quad (3)$$

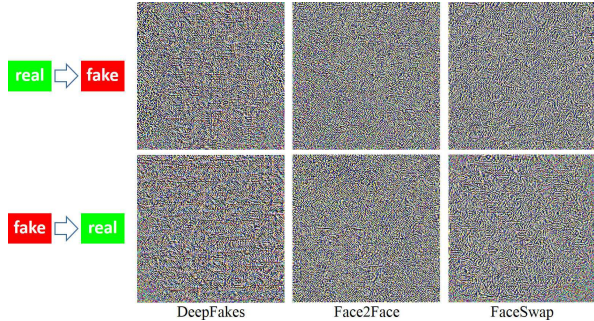


Fig. 3. UAPs (min-max scaled for display) generated for fabricating classification outputs.

Table 3. Performance of UAPs: image-agnostic property and transferability across unseen datasets.

	RMSE	acc (%) for FFM [12]			average drop
		DeepFakes	Face2Face	FaceSwap	
original	-	94.79	91.86	89.29	91.98
URN	2.17	87.21	74.64	80.25	11.28↓
DeepFakes	2.13	0.54	54.93	60.00	33.63↓
Face2Face	2.16	66.04	6.96	55.86	88.81↓
FaceSwap	2.05	62.11	51.18	2.00	3.17

Clearly, minimizing the objective function in Eq.(2) is equivalent to maximizing $a_{i,c}$. At the beginning of the iteration procedure, both $a_{i,c}$ and $a_{i,1-c}$ are small, and we have $a_{i,c} \approx a_{i,1-c}$ in most cases. If we set $\kappa > 1.0$, the exponential term in Eq.(2) can amplify the difference between $a_{i,c}$ and $a_{i,1-c}$ so as to initially provide a sufficient loss. After several iterations, the value of the exponential term approaches 1 while the negative term becomes a potency to further minimize the loss.

Only 280 iterations were needed to generate an effective UAP in our experiments, which were performed in a data-free manner. This demonstrates that over-firing is a resource-conserving approach for attackers. Looking at the generated UAPs in Fig.3, we observe similar local textures organized with different styles. For each dataset, two UAPs which can over-fire the two disjoint zones, are crafted separately. As shown in Table 3, classification accuracy was reduced on average from 91.98% (orange shading) to 3.17% (blue shading), which demonstrates the image-agnostic property of UAPs. Evaluation of transferability across unseen datasets showed that adding UAPs reduced accuracy 33.63% on average (gray shading). As a reference, uniform random noises (URNs) with the same level of strength only achieved a slight drop of 11.28% (green shading).

UAP transferability across unseen models is highly desirable, especially when the adversary has no knowledge of such models. The UAPs computed for the FFM [12] directly transfer to attack other target FFMs [10, 11]. Table 4 shows the evaluation results (brown ink for [11]). Note that the FFM [11] is reimplemented here without including the residual module. As shown in Table 4, the UAPs

reduced average accuracies by 19.19% and 24.06%, respectively, for the two unseen FFMs. Again, the UAPs outperform the URNs, which demonstrates that an adversarial attack based on over-firing can probe special noise patterns that contaminate the learned features even though the network architectures differ. Interestingly, if we retain the residual module for the FFM [11], the UAPs and URNs have comparable performance, i.e., an average drop of around 30% (not shown in Table 4). The reasons for this are twofold. First, the residual module extracts high-frequency details, which renders the

Table 4. Performance of UAPs: transferability across unseen FFMs.

	RMSE	acc (%) for FFMs [10,11]			average drop	
		DeepFakes	Face2Face	FaceSwap		
original	-	96.18	95.18	93.29	94.88	
	-	88.46	85.82	84.89	86.39	
URN	2.17	86.71	91.07	88.54	6.11↓	
	2.17	87.32	70.04	76.04	88.77	
UAP	DeepFakes	2.13	75.54	82.43	71.96	8.59↓
		2.13	73.11	66.29	50.86	77.80
	Face2Face	2.16	76.57	83.64	70.43	19.19↓
		2.16	73.04	64.39	51.93	75.69
	FaceSwap	2.05	78.14	72.03	70.50	24.06↓
		2.05	66.96	68.54	45.86	62.33

Table 5. Results of subjective assessment.

	IAP	UAP	URN	baseline
averaged score	3.45	4.21	4.39	4.49

whole model sensitive to both kinds of perturbations. Second, the residual maps may lie in a region far from the manifold of original data, so transferability is no longer effective.

3.3. Subjective assessment

Imperceptibility is an essential requirement for adversarial perturbations. However, the objective criteria like RMSE can not dutifully reflect the perceptual loss caused by local but condensed distortions. We conducted subjective assessment for the visual quality of adversarial images by using the degradation category rating method [20]. We asked evaluators to compare a clean image with its noisy version and then to rate the quality degradation on a 5-point mean opinion score scale, with 5 being the least degradation. We selected IAPs (all groups of ‘20 iters’), UAPs and URNs as the distortion sources, and compared the clean image with itself as a baseline. As such, there were four conditions, each consisting of 300 pairs selected at random. We exhibited some pairs at <https://nii-yamagishilab.github.io/Samples-Rong/Image-AE-attack/>.

The evaluation was performed through a web-based interface, with each web page horizontally displaying a pair of images. We grouped 21 pairs into a set, and each evaluator was permitted to evaluate at most 5 sets. We collected a total of 39680 legitimate scores from 775 evaluators. As shown in Table 5, the UAP and URN scores were comparable and close to baseline 4.49. This demonstrates that UAPs are visually negligible. The lower IAP score suggests that local but condensed distortions are prone to serious perceptual losses. Therefore, future work on individual adversarial attacks should enforce a constraint based on local smoothness.

4. CONCLUSION

Our study had demonstrated the existence of adversarial perturbations for FFMs. The gradient-based iterative procedure generates IAPs that can be used to fabricate classification and segmentation outputs. Without the need for training data, UAPs are crafted to over-fire the latent neurons. The objective function we designed provides a sufficient initial loss, which makes the over-firing practical with lightweight computational cost. Our experiments demonstrated that UAPs have transferability across unseen datasets and unseen FFMs, and our subjective assessment showed that the distortions incurred

by UAPs are visually negligible. This work can serve as a baseline for evaluating the adversarial security of FFMs. Future work includes developing a defense module that can protect FFMs against adversarial attacks.

5. REFERENCES

- [1] <https://github.com/deepfakes/faceswap/>
- [2] <https://github.com/MarekKowalski/FaceSwap/>
- [3] P. Korshunov, S. Marcel, "Speaker Inconsistency Detection in Tampered Video," in *Proc. 26th Eur. Signal Process. Conf. (EUSIPCO)*, pp.2375-2379, 2018.
- [4] Y. Li, M.C. Chang, S.W. Lyu, "In Ictu Oculi: Exposing AI Generated Fake Face Videos by Detecting Eye Blinking," in *Proc. IEEE Int. Workshop Inform. Forensics Secur. (WIFS)*, pp.1-7, 2018.
- [5] X. Yang, Y.Z. Li, S.W. Lyu, "Exposing Deep Fakes Using Inconsistent Head Poses," in *Proc. 44th IEEE Int. Conf. Acoust., Speech, Signal Process. (ICASSP)*, pp.8261-8265, 2019.
- [6] D. Wen, H. Han, A.K. Jain, "Face Spoof Detection with Image Distortion Analysis," *IEEE Trans. Inform. Forensics Secur.*, 10(4):746-761, 2015.
- [7] H.D. Li, B. Li, S.Q. Tan, J.W. Huang, "Detection of Deep Network Generated Images Using Disparities in Color Components," *arXiv preprint:1808.07276v2*, 2019.
- [8] Y.Z. Li, S.W. Lyu, "Exposing DeepFake Videos by Detecting Face Warping Artifacts," in *Proc. 2019 IEEE Conf. Comput. Vis. Pattern Recogn. Workshop (CVPRW)*, pp.46-52, 2019.
- [9] H.X. Mo, B.L. Chen, W.Q. Luo, "Fake Faces Identification via Convolutional Neural Network," in *Proc. 6th ACM Workshop Inform. Hiding & Multimedia Secur. (IH&MMSec)*, pp.43-47, 2018.
- [10] D. Afchar, V. Nozick, J. Yamagishi, I. Echizen, "MesoNet: A Compact Facial Video Forgery Detection," in *Proc. IEEE Int. Workshop Inform. Forensics Secur. (WIFS)*, pp.1-7, 2018.
- [11] D. Cozzolino, J. Thies, A. Rössler, C. Riess, M. Nießner, L. Verdoliva, "ForensicTransfer: Weakly-Supervised Domain Adaptation for Forgery Detection," *arXiv preprint:1812.02510v1*, 2018.
- [12] H.H. Nguyen, F.M. Fang, J. Yamagishi, I. Echizen, "Multi-task Learning for Detecting and Segmenting Manipulated Facial Images and Videos," *Proc. 10th IEEE Int. Conf. Biom. Theory, Appl. Syst. (BTAS)*, pp.1-8, 2019.
- [13] N. Akhtar, A. Mian, "Threat of Adversarial Attacks on Deep Learning in Computer Vision: A Survey," *IEEE Access*, 6:14410-14430, 2018.
- [14] X.Y. Yuan, P. He, Q.L. Zhu, X.L. Li, "Adversarial Examples: Attacks and Defenses for Deep Learning," *IEEE Trans. Neural Net. Learn. Syst.*, 30(9):2805-2824, 2019.
- [15] M. Sharif, S. Bhagavatula, L. Bauer, M. K. Reiter, "Accessorize to a Crime: Real and Stealthy Attacks on State-of-the-Art Face Recognition," *Proc. ACM SIGSAC Conf. Comput. Commun. Secur.*, pp.1528-1540, 2016.
- [16] C.H. Xie, J.Y. Wang, Z.H. Zhang, Y.Y. Zhou, L.X. Xie, A. Yuille, "Adversarial Examples for Semantic Segmentation and Object Detection," *Proc. Int. Conf. Comput. Vis. (ICCV)*, pp.1378-1387, 2017.
- [17] J.H. Metzen, M. C. Kumar, T. Brox, V. Fischer, "Universal Adversarial Perturbations Against Semantic Image Segmentation," *Proc. IEEE Conf. Comput. Vis. Pattern Recognit. (CVPR)*, pp.2755-2764, 2017.
- [18] R. Jia, P. Liang, "Adversarial Examples for Evaluating Reading Comprehension Systems," *Proc. Conf. Empirical Methods Natural Lang. Process. (EMNLP)*, pp.2021-2031, 2017.
- [19] K. Grosse, N. Papernot, P. Manoharan, M. Backes, P. McDaniel, "Adversarial Examples for Malware Detection," *Proc. Eur. Symp. Res. Comput. Secur. (ESORICS)*, pp.62-79, 2017.
- [20] ITU-R Recommendation BT.1866, "Objective Perceptual Video Quality Measurement Techniques for Broadcasting Applications Using Low Definition Television in the Presence of a Full Reference Signal," 2010.
- [21] A. Rössler, D. Cozzolino, L. Verdoliva, C. Riess, J. Thies, M. Nießner, "FaceForensic++: Learning to Detect Manipulated Facial Images," *arXiv preprint:1901.08971v3*, 2019.
- [22] C. Szegedy, W. Zaremba, I. Sutskever, J. Bruna, D. Erhan, I. Goodfellow, R. Fergus, "Intriguing Properties of Neural Networks," *arXiv preprint:1312.6199v4*, 2014.
- [23] I. Goodfellow, J. Shlens, C. Szegedy, "Explaining and Harnessing Adversarial Examples," *arXiv preprint:1412.6572v3*, 2015.
- [24] A. Kurakin, I. Goodfellow, S. Bengio, "Adversarial Examples in the Physical World," *arXiv preprint:1607.02533v4*, 2017.
- [25] S. Moosavi-Dezfooli, A. Fawzi, P. Frossard, "DeepFool: A Simple and Accurate Method to Fool Deep Neural Networks," *Proc. 2016 IEEE Conf. Comput. Vis. Pattern Recogn. (CVPR)*, pp.2574-2582, 2016.
- [26] S. Moosavi-Dezfooli, A. Fawzi, O. Fawzi, P. Frossard, "Universal Adversarial Perturbations," *Proc. 2017 IEEE Conf. Comput. Vis. Pattern Recogn. (CVPR)*, pp.86-94, 2017.
- [27] K. Mopuri, A. Ganeshan, R. Babu, "Generalizable Data-Free Objective for Crafting Universal Adversarial Perturbations," *IEEE Trans. Pattern Anal. Mach. Intell.*, 41(10):2452-2465, 2019.